# State Estimation of Terrestrial and Space Based Passive RF Architectures for Use in Cislunar SSA Utilizing Existing SSN Locations

**Kullen Waggoner**
*Air Force Institute of Technology*
**David Curtis**
*Air Force Institute of Technology*

## ABSTRACT

This paper explores and analyzes the use of a network of terrestrial and the potential addition of a space-based RF receiver to conduct Space Situational Awareness (SSA) in cislunar space using passive Time Difference of Arrival (TDOA) and Frequency Difference of Arrival (FDOA) measurements. First, this paper explores the use of terrestrial architectures that utilize preexisting Space Surveillance Network (SSN) locations and identifies the best configuration for each based on the potential geometric dilution of precision (GDOP) and line-of-sight (LOS) availability. This analysis shows points of minimal return where the addition of more ground stations does not appreciably improve state estimation. Next, a demonstration shows that cislunar SSA state estimation accuracy for both batch estimation and sequential estimation improves as GDOP decreases and LOS improves. Finally, this paper models and simulates the accuracy of a ground-only and a GEO-augmented Passive RF system, demonstrating nearly an order of magnitude increase in accuracy with a single satellite.

## 1. INTRODUCTION

Fundamental to SSA is the use of some type of measurements to estimate a space object's position and velocity states as well as the associated uncertainty covariance. This estimate enables the prediction of the future position of the object for general awareness and collision avoidance. Over the last 50 years, the US Air Force, then superseded by the US Space Force, developed the SSN to provide military and civilian SSA to the US and its allies. The SSN is a widespread network of electro-optical telescopes and radar sites that enables the sharing of SSA information. This data is in the form of two-line element (TLE) sets for objects as small as a softball, and its coverage extends from low-earth orbit (LEO) to geosynchronous orbits (GEO). Within the last ten years, planned and executed missions to areas of space beyond the GEO belt and moon have increased substantially. As a result of the increase in cislunar activity, a need for SSA in this regime also increased. Expanding SSA into the large cislunar regime presents several challenges as the volume of space and distances in this region are much greater than the near-earth orbital regimes. The moon is over ten times farther from the earth than a satellite in GEO. Electro-optical and radar measurements are somewhat limited in their effectiveness due to these large distances as well as significant solar/lunar exclusion zones [1]. These circumstances provide an opportunity to rethink and explore less-frequently used methods to solve this estimation problem such as passive RF to measure satellite locations. Within the existing literature, passive RF has been shown to provide robust SSA information for near-earth objects [2,3]. Further work showed the feasibility and the potential advantages of using a passive TDOA and FDOA SSA architectures both as a standalone measurement technique [4,5] and in conjunction with other measurement phenomenologies for cislunar [6]. Unlike electro-optical systems, illumination and light saturation are not factors for passive RF; additionally, signal loss is significantly less than radar systems over cislunar distances. This paper explores and simulates the reception of modulated signals received at multiple receivers to acquire the characteristic TDOA/FDOA measurements. It uses circularly restricted three-body problem dynamics (CR3BP) to model the movement of the space objects in cislunar and near-earth regimes.

## 2. BACKGROUND

### 2.1 Passive RF Measurements

The passive RF measurements modeled in this paper consist of TDOA and FDOA. TDOA is a measurement of the difference in the signal delay from an emitter as measured at two or more separate receivers. As shown in this paper, the receivers can be either space-based or ground-based. The delay ($\tau$) is directly related to the difference in the relative range between each receiver and the emitter and inversely proportional to the propagation velocity or speed

of light for RF signals ($c$) [7,8]. Assuming the relative position of the emitter with respect to the sensors is $\boldsymbol{\rho_i}$, then the measurement function for TDOA becomes:

$$G_{TDOA} = [\tau] = \frac{1}{c}[\|\boldsymbol{\rho_2}\| - \|\boldsymbol{\rho_1}\|] \tag{1}$$

FDOA measures the difference in arrival frequency from the emitter to two or more sensors. The difference in the arrival frequency is caused by the different Doppler shifts of the emitted signal to each receiver. FDOA is directly related to the difference in the relative radial velocity or range-rate of each receiver to the emitter [7,8]. For the FDOA measurement equation shown below, $\boldsymbol{v_e}$ and $\boldsymbol{v_i}$ represent the emitter velocity and the sensor velocities, respectively, and $f_0$ represents the signal carrier frequency.

$$G_{FDOA} = [\Delta f] = \frac{f_0}{c}\left(\left(\frac{\boldsymbol{\rho_2}}{\|\boldsymbol{\rho_2}\|}\right)^T(\boldsymbol{v_e} - \boldsymbol{v_2}) - \left(\frac{\boldsymbol{\rho_1}}{\|\boldsymbol{\rho_1}\|}\right)^T(\boldsymbol{v_e} - \boldsymbol{v_1})\right) \tag{2}$$

To simulate the TDOA/FDOA measurements for use in modeling and simulation within this paper, the measurement equations (Equation 1 and 2) are used and additive white gaussian noise is added to simulate a noisy non-perfect measurement. The standard deviation noise levels of the additive white noise for all simulations are $\sigma_{TDOA} = 10nsec$, $\sigma_{FDOA}$ = 0.01 Hz. The carrier frequency modeled is 4.0 GHz and is known to the receivers. Noise values are based on values used in similar research efforts [5,9]. Finally, for modeling purposes, 200 evenly spaced passive RF collection opportunities are provided within each estimation scenario. Each scenario runs for a full period of the emitter as explained in the next sections.

### 2.2 CR3BP Dynamics and Periodic Orbits

Circularly restricted three-body problem (CR3BP) dynamics are used first for creating and simulating the cislunar environment. The same dynamics are also used for creating simulated measurement data and the propagation of states within the batch and sequential estimators. The common assumptions and setup associated with the CR3BP are utilized including the use of a rotating synodic frame; use of non-dimensional mass, length, and time parameters; assumption of a circular orbit of the moon around the earth and ignoring all other perturbing forces [10,11]. The relative equations of motion (EOMs) are provided below in Equations 3-5 and the potential function is provided in Equation 6. A more thorough derivation and development of the CR3BP assumptions and EOMs can be found in Parker and Anderson's book [12].

$$\ddot{x} - 2\dot{y} = \frac{\partial U}{\partial x} \tag{3}$$

$$\ddot{y} + 2\dot{x} = \frac{\partial U}{\partial y} \tag{4}$$

$$\ddot{z} = \frac{\partial U}{\partial z} \tag{5}$$

$$U(x, y, z) = \frac{1}{2}(x^2 + y^2) + \frac{1-\mu}{\rho_1} + \frac{\mu}{\rho_2} \tag{6}$$

Periodic planar and out-of-plane orbits are used to simulate the trajectory of the emitter object for each model scenario. Figure 1 shows plots of all seven of the emitter orbits referenced in the analysis and results sections. As is seen, periodic orbits within the synodic frame and under CR3BP assumptions do not follow traditional two-body Keplerian conic sections. In fact, they are not perfectly periodic and will tend to diverge, sometimes quickly after only a couple periods due to the instability and chaotic nature of CR3BP dynamics. To create each of the seven closed trajectories, various methods are used including: a two-level corrector [13] for the L1 Lyapunov and L2 Lyapunov, a simple corrector [14] for the L4 Lyapunov and both halo orbits, and Poincaré mapping [15,16] to find the resonant orbit. The periods of the orbits vary from 4.2 days for the resonant orbit to 28.6 days for the planar orbit about the L4 point. Each trajectory is simulated using only CR3BP dynamics. No perturbing or control forces are applied during the simulations.

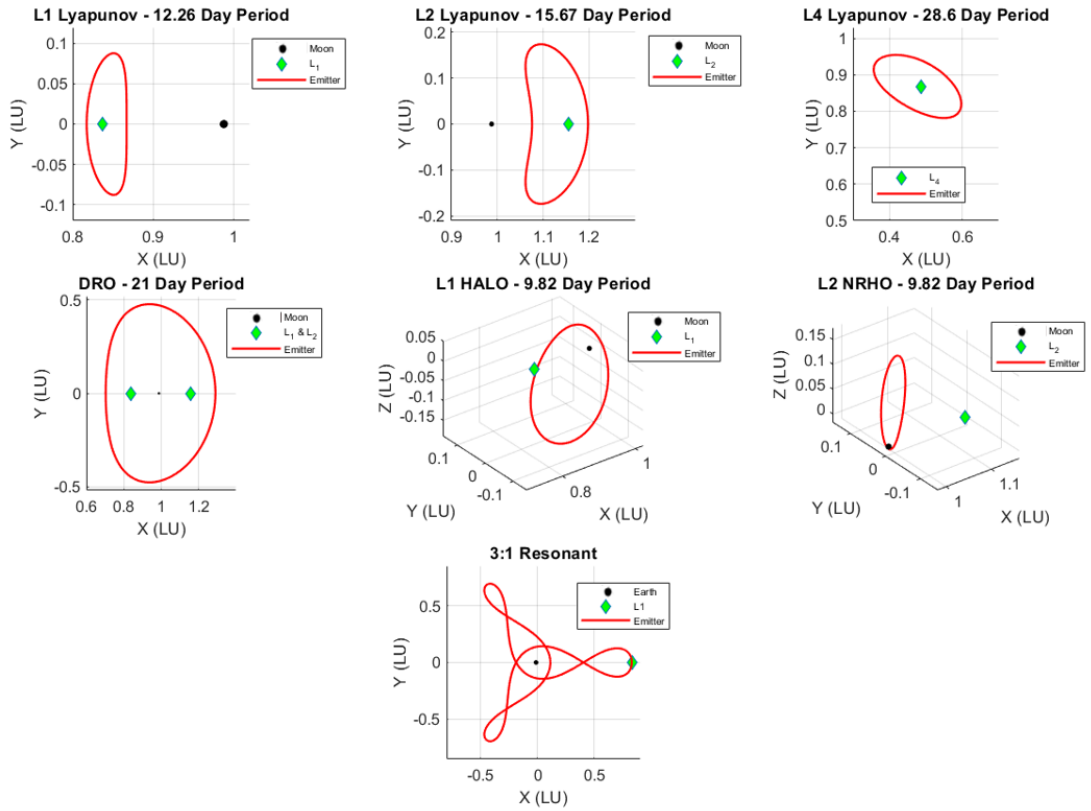


Fig. 1. Seven closed periodic orbits created using CR3BP dynamics and assumptions. All are shown within the rotating earth-moon frame. Dimensions are CR3BP units in which 1 LU = 384,400 km.

### 2.3 TDOA and FDOA GDOP

GDOP is a metric used to evaluate the configuration and location of the receivers and emitters and determine how that arrangement will affect the accuracy of the state estimate. A lower GDOP is more desirable as it generally indicates lower errors in the estimated final position states. GDOP is widely used throughout the Global Navigation Satellite System (GNSS) community to provide insight into alignment of satellites and what position and timing accuracy is to be expected from that alignment. Fundamentally, the GDOP is the ratio of the RMS position error to the RMS ranging error as shown in Equation 7. $Var(e_i)$ represents the statistical variance of the estimated position error $(e_i)$ and $Var(Z)$ represents the expected variance in the measurements.

$$GDOP = \sqrt{\frac{Var(e_x) + Var(e_y) + Var(e_z)}{Var(Z)}} \tag{7}$$

After linearization and allowing for the combination of multiple measurement types (TDOA and FDOA), the GDOP simplifies into Equation 8. A further discussion and demonstration of the derivation of GDOP for combining multiple measurement types is provided by [17].

$$GDOP = \sqrt{trace(H^T W H)^{-1}} \tag{8}$$

The matrix $H$ represents the Jacobian of the measurement function (Equation 9) and $W$ represents a square diagonal weighting matrix comparing the measurement uncertainty of the TDOA to the FDOA (Equation 10). When combining $n$ number of TDOA/FDOA measurements simultaneously from multiple receiver pairs, the $H$ matrix grows vertically, adding new rows for each new pair. The weighting matrix grows along the diagonal [17]. The units for the GDOP are distance per unit of measurement. For the case of using GDOP for estimation using only TDOA, the units are distance per time, and the GDOP for estimation with only FDOA is distance per frequency.

The combined estimation using both TDOA and FDOA could be accomplished using either unit depending on the derivation of the combined GDOP. For the derivation utilized in this paper, the weighting matrix and Equation 7 are defined such that the final GDOP is in units of distance per time or km/nsec for convention.

$$H = \begin{bmatrix} \frac{\partial G_{TDOA_1}}{\partial x} & \frac{\partial G_{TDOA_1}}{\partial y} & \frac{\partial G_{TDOA_1}}{\partial z} \\ \frac{\partial G_{FDOA_1}}{\partial x} & \frac{\partial G_{FDOA_1}}{\partial y} & \frac{\partial G_{FDOA_1}}{\partial z} \\ \vdots & \vdots & \vdots \\ \frac{\partial G_{TDOA_n}}{\partial x} & \frac{\partial G_{TDOA_n}}{\partial y} & \frac{\partial G_{TDOA_n}}{\partial z} \\ \frac{\partial G_{FDOA_n}}{\partial x} & \frac{\partial G_{FDOA_n}}{\partial y} & \frac{\partial G_{FDOA_n}}{\partial z} \end{bmatrix} \tag{9}$$

$$W = \sigma_{TDOA}^2 \begin{bmatrix} 1 & 0 & 0 & 0 & 0 \\ 0 & \frac{\sigma_{FDOA}^2}{\sigma_{TDOA}^2} & 0 & 0 & 0 \\ \vdots & \vdots & \ddots & \vdots & \vdots \\ 0 & 0 & 0 & 1 & 0 \\ 0 & 0 & 0 & 0 & \frac{\sigma_{FDOA}^2}{\sigma_{TDOA}^2} \end{bmatrix} \tag{10}$$

A breakdown of the combined GDOP, TDOA GDOP, and FDOA GDOP is provided in Figure 2. GDOP is highly bimodal. The GDOP solutions are clustered at around either 1 km/nsec or $10^7$ km/nsec. Figure 2 shows in physical terms what causes the jump between the two regimes. When many pairs of receivers are in view, then in general, the GDOP will cluster near the $10^0$-$10^1$ km/nsec as the solution is generally fairly strong. However, if few pairs are in view, then the matrix multiplication ($H^T W H$) becomes badly conditioned or near singular, causing the GDOP to jump.

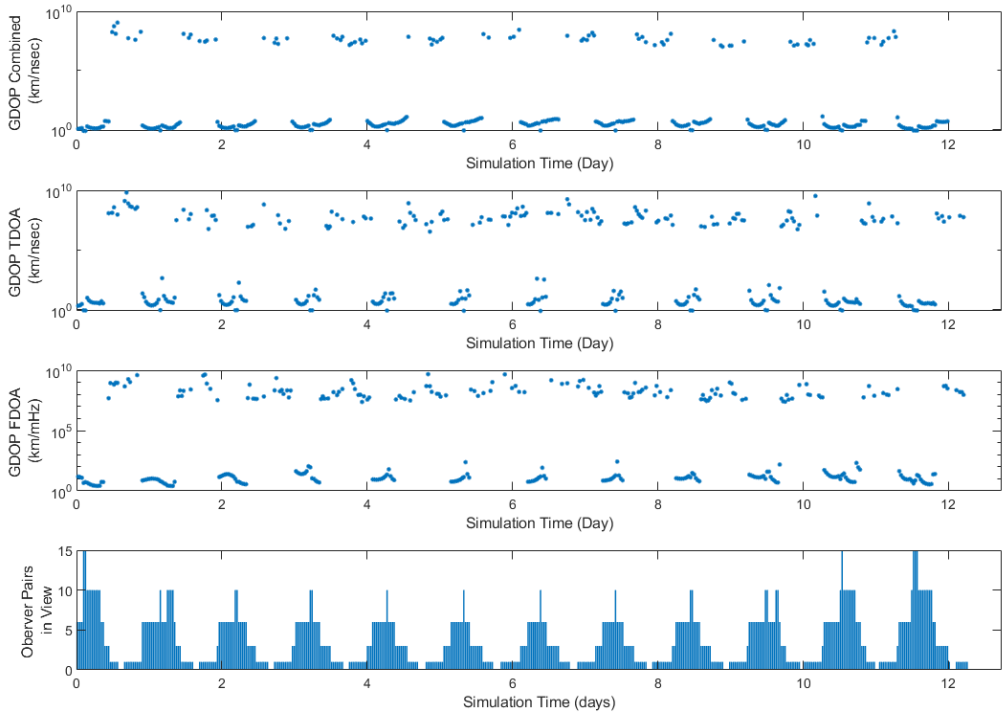


Fig. 2. GDOP for combined TDOA/FDOA, TDOA-only and FDOA-only for an L1 Lyapunov scenario using six ground receivers. The bottom plot shows the instantaneous number of pairs of receivers in view throughout the scenario.

### 2.4 Space Force Space Surveillance Network

The SSN is a network of globally distributed sensors for the purpose of tracking and cataloging both active and non-active earth-orbiting satellites. The network takes many measurements of space objects and compiles them to create a catalog published as TLE's from the Combined Space Operations Center (CSpOC). The United States' SSN was developed out of the Cold War's ballistic-missile warning radar and tracking assets and is therefore biased towards locations better for missile warning and not locations that would be ideal for space tracking. This includes significant assets at high northern latitudes and near US coastal regions. The SSN dedicated and collateral sensors include radar, phased array, and optical systems including the Ground-based Electro-Optical Deep Space Surveillance (GEODSS) system. This research utilizes SSN locations as published by NASA and within the published literature [11,18] as candidate locations for use in a potential passive RF cislunar SSA system. Locations utilized are shown in Figure 3 and are provided in Table 1.

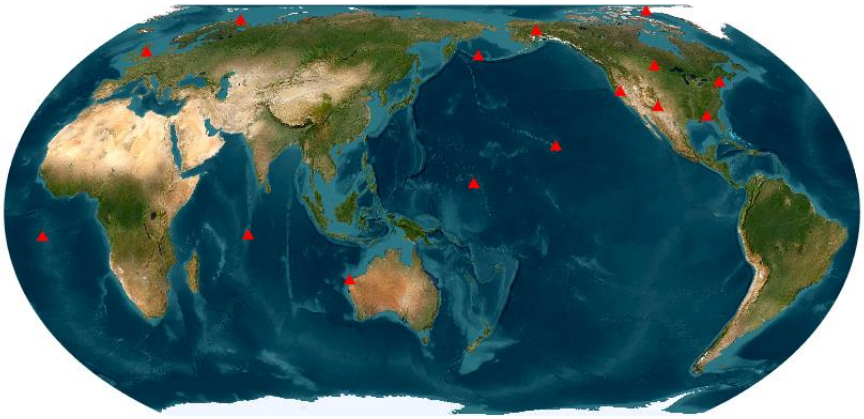

Fig. 3. Red triangles represent sites analyzed for ground receiver locations for a passive RF cislunar network based on existing and historical SSN dedicated, collateral, and contributing sensors [11].

Table. 1. Latitude and Longitude for SSN dedicated, collateral, and contributing sensors as of 2020 [11,18].

| Number | Site | Latitude | Longitude |
|---|---|---|---|
| 1 | Socorro, NM | 33.82 | -106.66 |
| 2 | Maui, HI | 20.71 | -156.26 |
| 3 | Diego-Garcia, Indian Ocean | -7.41 | 72.45 |
| 4 | Eglin, FL | 30.57 | -86.21 |
| 5 | GLOBUS, Norway | 70.37 | 31.13 |
| 6 | Kwajalein, Pacific Ocean | 8.72 | 167.72 |
| 7 | Holt, Australia | -21.82 | 114.17 |
| 8 | Ascension, Atlantic Ocean | -7.91 | -14.40 |
| 9 | Beal, CA | 39.14 | -121.35 |
| 10 | Cavalier, ND | 48.72 | -97.90 |
| 11 | Clear, AK | 64.29 | -149.19 |
| 12 | Boston, MA | 42.62 | -71.49 |
| 13 | Flyingdales, UK | 54.37 | -0.67 |
| 14 | Pituffik (Thule), Greenland | 76.57 | -68.30 |
| 15 | Cobra Dane, AK | 52.74 | 174.09 |

## 3. ANALYSIS AND RESULTS

### 3.1 Predicted GDOP of SSN for Cislunar Passive RF Estimation

The first evaluation of potential passive RF locations includes finding GDOP and line-of-sight (LOS) limitations of different selections of existing SSN sites. The LOS percentage is defined as the percentage of simulation time steps in which at least a single pair or receivers each have a line-of-sight to the emitting satellite unobscured by either the surface of the earth or the moon. Figure 4 shows the results of simulations in which an L1 planar Lyapunov orbit is

simulated throughout one 12.26-day period. Each potential permutation of the fifteen receiver stations listed in Table 1 and is evaluated to find the GDOP at 100 equally spaced discrete time throughout the simulation. A scaled down plot showing only the results from 2, 5, 8, 11, and 14 receiver permutations are shown in Figure 4. As can be seen, some interesting results jump out. These include that the selection of sites can significantly impact median GDOP, especially satellite configurations with five or less receiver sites. Additionally, the best potential GDOP for the modeled TDOA/FDOA measurement accuracy is generally between 1 km/nsec and 10 km/nsec. As the GDOP asymptotically approaches this limit for terrestrial based receivers against a cislunar target emitter, the addition of ground stations does not significantly improve the GDOP but instead improves the LOS availability percentage for a given architecture.

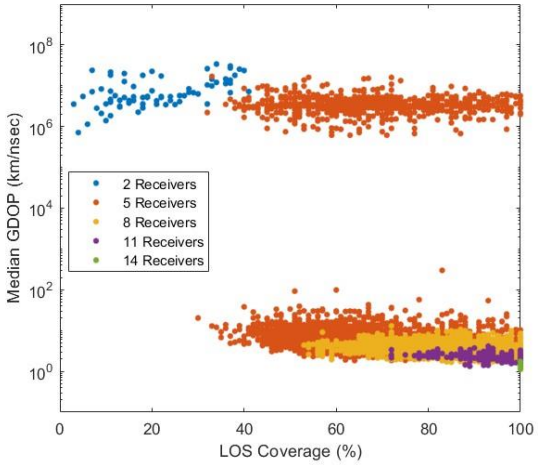


Fig. 4. Median GDOP throughout simulation for each permutation of ground stations for measurement of L1 Lyapunov emitter satellite. Simulation length was one period (12.6 days). Terrestrial only networks show a maximum predicted GDOP between 1km/nsec to 10 km/nsec.

The next step of GDOP analysis (Figure 5) looked at a zoomed-in portion of the above plot to find a potential point of diminishing returns for the improvement of median GDOP as opposed to the addition of ground sites. As can be seen, after the creation of an architecture of five or six selectively chosen ground stations, the addition of more ground stations will not significantly improve the LOS coverage or the median GDOP for passively observing objects around L1.

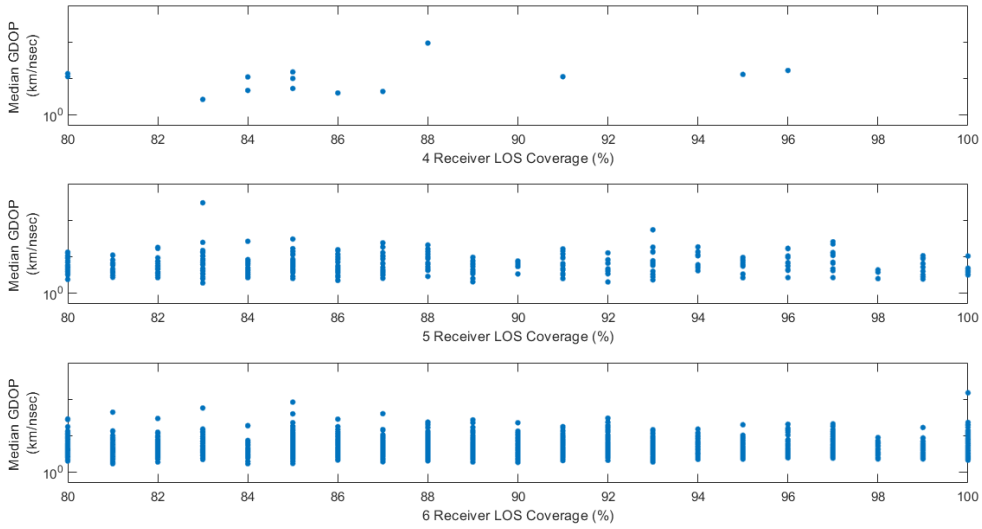


Fig. 5. Median GDOP and line-of-site coverage throughout simulation for each permutation of four, five, and six ground stations for measurement of an L1 Lyapunov emitter satellite. Simulation length was one period (12.6 days).

### 3.2 Least-Squares Estimate of Cislunar Object Using Ground Stations Only

A simulated batch least squares estimation (LSE) as detailed in a previous paper [4]using different combinations of receivers was accomplished and the results are provided in Figure 6. Within each combination, a configuration corresponding to the optimal line-of-sight and GDOP were chosen for the estimation. The selected best configurations as well as the corresponding LOS percentage and median GDOP are provided in Table 2. For simulation purposes, multiple non-maneuvering emitter orbits throughout cislunar space were chosen as targets including a distant retrograde orbit (DRO), an L1 planar orbit with a period of 12.6 days, a L2 near-rectilinear halo orbit with a period of 5.96 days and a 3:1 resonant orbit. Overall, results from the LSE show that as expected, lower median GDOP is indicative of a way to lower the batch LSE estimation error throughout the trajectory. The resonant orbit had the lowest GDOP values because it has the closest approach to the earth of all the modeled orbits.

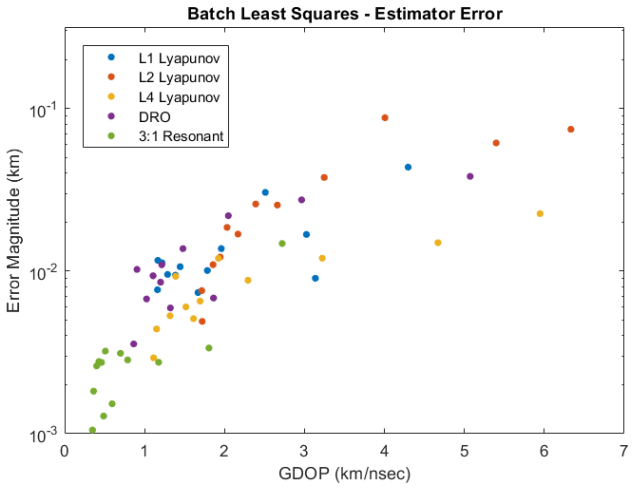


Fig. 6. Comparison of the median error of the batch least squares estimate of planar cislunar orbits as compared to the median GDOP using terrestrial-only receiver configurations using the best three station configuration through the best fifteen station configuration as provided by Table 2.

Table. 2. Best predicted configurations and measured performance based on analysis from Figure 4 for three through fifteen node terrestrial only passive RF architectures.

| Total Receievers | LOS | Median GDOP | Locations |
|---|---|---|---|
| 3 | 54% | 2.470 | Diego Garcia, Kwajalein, Holt |
| 4 | 87% | 4.359 | Maui, Diego Garcia, Kwajalein, Beale |
| 5 | 100% | 3.117 | Diego Garcia, Eglin, Kwajalein, Holt, Beale |
| 6 | 100% | 2.113 | Diego Garcia, Eglin, Holt, Ascension, Fylingdales, Thule |
| 7 | 100% | 1.876 | Diego Garcia, Kwajalein, Holt, Ascension, Beale, Fylingdales, Cobra Dane |
| 8 | 100% | 1.653 | Maui, Diego Garcia, Eglin, Holt, Ascension, Beale, Fylingdales, Cobra Dane |
| 9 | 100% | 1.436 | Maui, Diego Garcia, Kwajalein, Holt, Ascension, Beale,Boston,Fylingdales, Cobra Dane |
| 10 | 100% | 1.350 | Socorro, Maui, Diego Garcia, Eglin, Kwajalein, Holt, Ascension, Cavalier, Fylingdales, Cobra Dane |
| 11 | 100% | 1.264 | Maui, Diego Garcia, Eglin, Kwajalein, Holt, Ascension, Beale, Cavalier, Boston, Fylingdales, Cobra Dane |
| 12 | 100% | 1.188 | Socorro, Maui, Diego Garcia, Eglin, Kwajalein, Holt, Ascension, Beale, Clear, Boston, Fylingdales, Cobra Dane |
| 13 | 100% | 1.150 | All except Cavalier and Thule |
| 14 | 100% | 1.121 | All except Thule |
| 15 | 100% | 1.121 | All listed |

Further sequential estimation was conducted using both an Extended Kalman filter (EKF) and Unscented Kalman filter (UKF) to determine if median GDOP was also predictive of sequential estimation accuracy. As can be seen in Figure 7, the EKF and UKF follow the same trend as the batch estimator in which as the GDOP increases, the median error of the estimation increases as well. This is true for both in-plane trajectories and out-of-plane trajectories. The sequential estimation has significantly larger errors than the batch estimator as the batch estimator uses all measurements simultaneously to iteratively find the trajectory that best fits all measurements. The

sequential filters take each data point and use the previous estimates of the states and covariance to sequentially predict the current states with consideration of the measurements. The difference between the batch estimators to the sequential estimators is approximately two to three orders of magnitude.

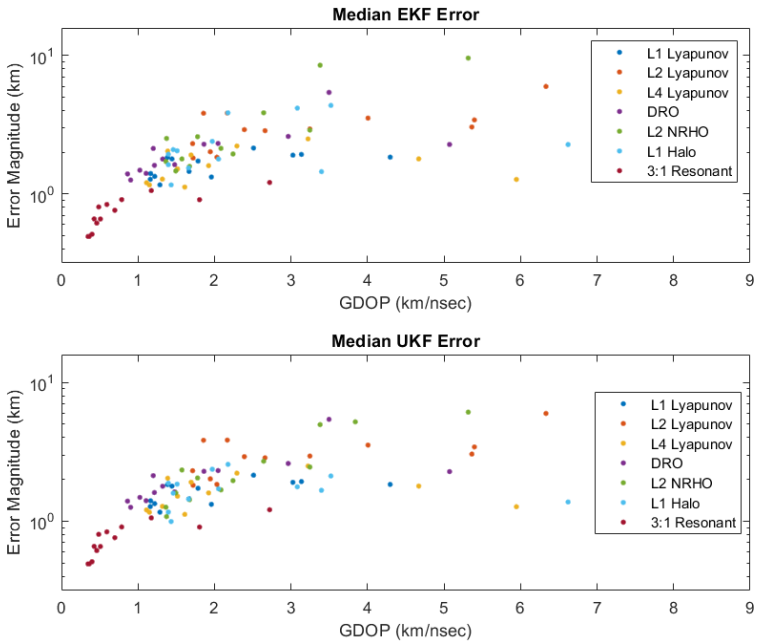


Fig. 7. This figure shows a comparison of the median error of the EKF (top) and UKF (bottom) for different in and out-of-plane cislunar orbits using terrestrial-only receiver configurations using the best three station configuration through the best fifteen station configuration as provided by Table 2.

The final analysis effort for the terrestrial-only stations examines and compares different numbers of observer receiver networks. Figure 8 and Figure 9 shows that after the use of six to eight ground stations, the addition of further ground stations, even if choosing the optimal placing does not appreciably improve estimator accuracy. To accomplish this analysis, batch least-squares estimates of the various planar orbits were conducted using the best demonstrated ground station architectures from Table 2. Comparing Figures 8 and 9 demonstrates that orbits and trajectories that are further away from the earth such as those around L2 or DROs where much of the orbit's period is spent on the other side of the moon, the point of minimal returns for the addition of ground stations is moved to the right and is closer to around eight or nine stations as can be seen in. This analysis shows similar results for a total of 356 repeated estimates for the L1 and L2 Lyapunov orbits in Figure 10.

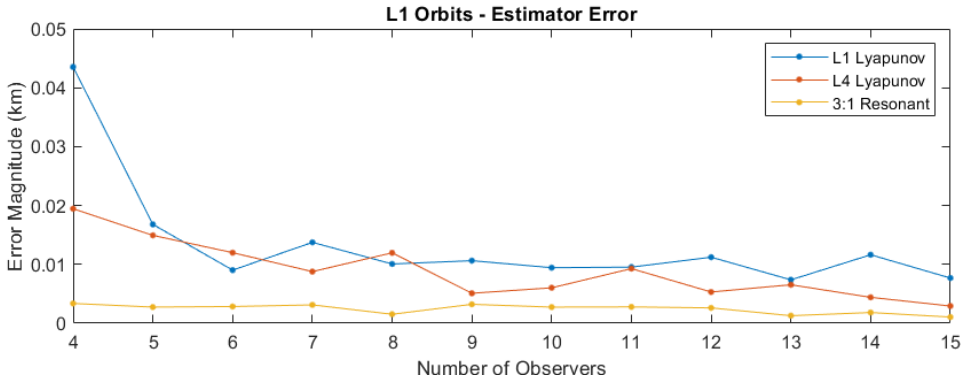


Fig. 8. This plot shows a comparison of the median error of the batch least squares estimate for in-plane orbits on the earth side of the moon showing marginal improvements in error reduction after six sites are used. The ground sites chosen are the configurations shown in Table 2.

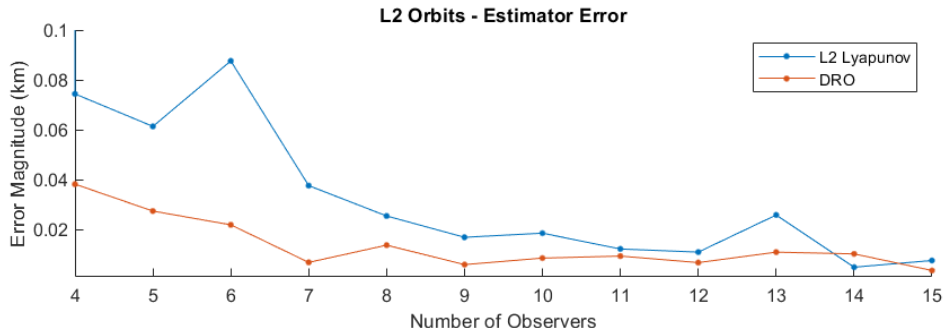


Fig. 9. This plot shows a comparison of the median error of the batch least squares estimate for in-plane orbits on the far side of the moon showing marginal improvements in error reduction after eight or nine sites are used. The ground sites chosen are the configurations shown in Table 2.

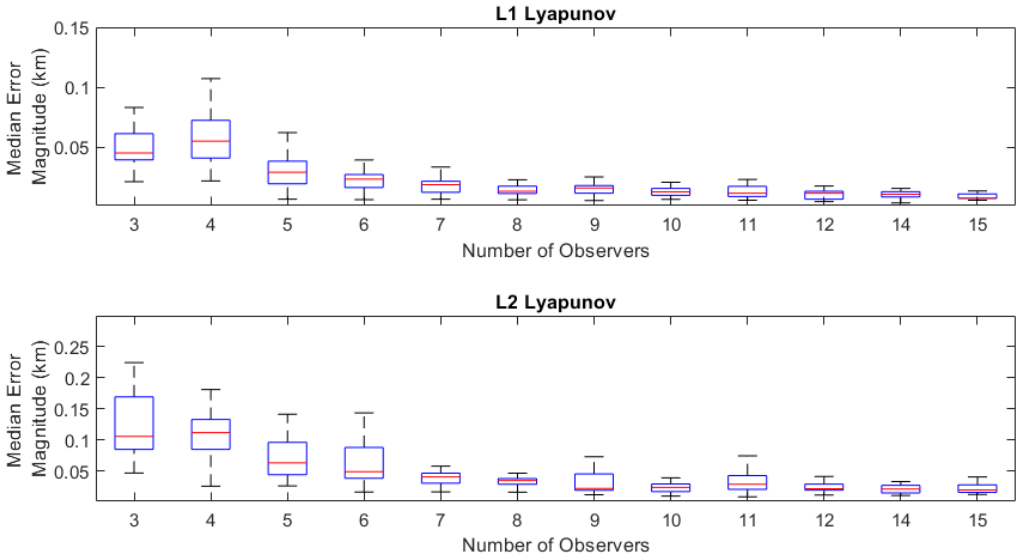


Fig. 10. Box and whisker plot showing the distribution of n = 356 batch least square estimates using optimally located ground networks (Table 2) from three to fifteen observers. Little improvement in error reduction is made after the addition of six or seven observers for the L1 emitter (top) and after seven or eight observers for the L2 emitter (bottom). The central mark indicates the median, and the bottom and top edges of the box indicate the 25th and 75th percentiles and the whiskers extend to the extrema of the data not considered outliers. Significant outliers indicating non-convergence of the LSE are omitted.

### 3.3 Hybrid Space-Augmented Ground Receiver Network

To improve the GDOP with the intent of refining the sequential and final batch estimate, the addition of a single satellite in LEO, medium earth orbit (MEO), highly elliptical orbit (HEO), or GEO is considered and added to the network simulation to determine what benefit it may provide. Figure 11 shows how the best permutation of the ground station receiver network from the analysis for Figure 4 could be improved by the addition of a single MEO, HEO, or GEO satellite, respectively. Figure 12 shows the results of a sequential state estimation of the L2 near-rectilinear halo orbit (NRHO) with and without the addition of a single GEO satellite. The results show that the addition of a single HEO or GEO satellite appears to most impactfully improve the GDOP performance. For architectures with only a few ground stations, the HEO satellite provided the best GDOP increase. For larger architectures, the GEO provided a larger improvement. This is somewhat to be expected as the HEO and GEO satellites have the highest orbital altitude of those modeled and it then reasons that GDOP will be most significantly improved. From Figure 11, it follows that the addition of a GEO or HEO satellite will improve the GDOP by approximately a full order of magnitude.

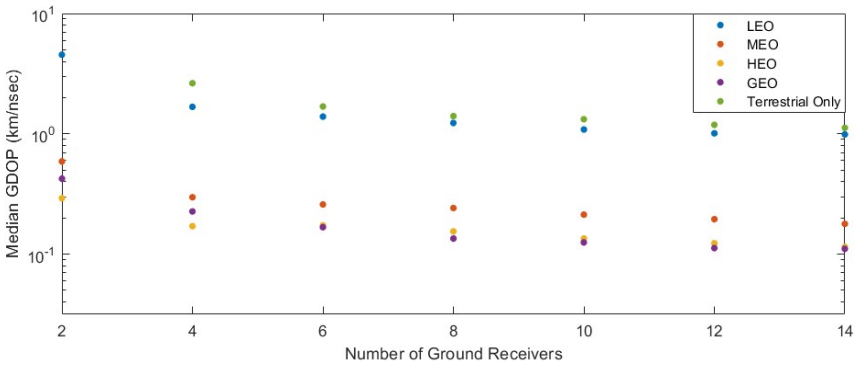


Fig. 11. Median GDOP throughout simulation for the best permutation of two through fourteen ground stations. Target satellite was an L1 Lyapunov emitter satellite. The addition of a HEO or GEO satellite shows an improvement in predicted GDOP of up to an order of magnitude.

A comparison of the errors from the sequential estimation for both the GEO-augmented and non-GEO augmented sequential estimation is provided in Figure 5. The addition of the single GEO satellite improved the median error throughout the whole simulation by nearly an order of magnitude demonstrating further that GDOP is in general a good predictor of the estimation accuracy of a given passive RF system. Additionally, the GEO-augmented architecture's LOS availability was 98.6% as opposed to the terrestrial only system in which the LOS availability was only 91.4%. The UKF performed slightly better than the EKF which is expected as the CR3BP dynamics, especially for an out-of-plane trajectory nearing the moon are highly non-linear. Finally, throughout the sequential estimation, the X-coordinate, which within the synodic frame represents the axis that connects the center of the earth to the center of the moon, has the highest error. This is somewhat in line with previously published literature [4,19] which has found the uncertainty within the cislunar frame is often largest in the direction corresponding to the X-axis.

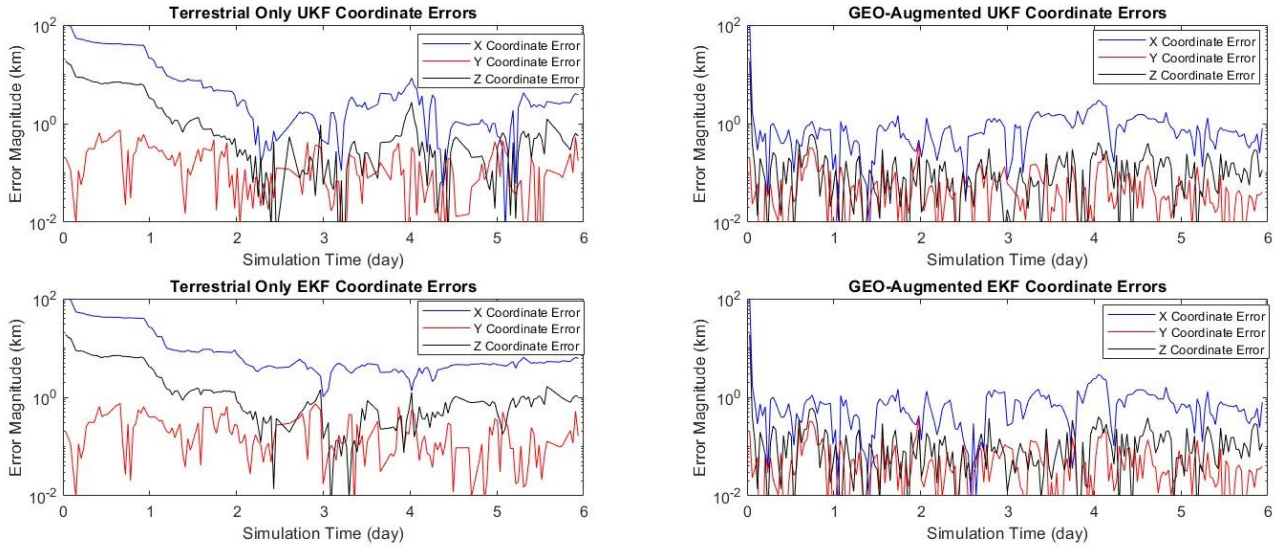


Fig. 12. Position coordinate errors for a UKF and an EKF for the L2 NRHO simulation with (left) a terrestrial-only six site architecture and (right) a six-station terrestrial based system with the addition of a single GEO satellite. Median error decreased for the EKF from 3.425 km to 0.505 km and for the UKF from 2.585 km to 0.491 km.

## 4. SUMMARY

This paper analyzes the use of existing and historical SSN sites as well as potential future space-based platforms for passive RF TDOA/FDOA-based cislunar orbit determination and state estimation. First, this paper demonstrates that

combined TDOA and FDOA GDOP is a simple metric that is useful for assessing the geometry of receivers for cislunar state estimation. Further, analysis of GDOP shows that proper site selection as well as the number of ground receivers are important for a passive RF architecture as they can significantly impact the estimation accuracy and LOS availability for cislunar SSA. These factors are the case for both batch and sequential estimation techniques. Additionally, this paper shows that the addition of a single space-based receiver satellite can improve the GDOP by an order of magnitude over terrestrial-only methods. GDOP analysis shows that the addition of a GEO satellite provides the greatest improvement of those modeled over the widest potential network applications. Finally, this paper demonstrates using a hybrid ground and space-based passive RF architecture for tracking with a sequential UKF and EKF of an L2 NRHO satellite, demonstrating a median error throughout the scenario of less than 0.5 km with LOS availability of 98.6%.

## 5. REFERENCES


[1] Frueh, C., Howell, K., Demars, K. J., and Bhadauria, S. "Cislunar Space Situational Awareness." *AAS/AIAA Space Flight Mechanics Meeting*, 2021.

[2] Shuster, S., Sinclair, A., and Lovell, T. A. "Initial Relative-Orbit Determination Using Heterogeneous TDOA." *IEEE Aerospace Conference Proceedings*, 2017.

[3] Christian, J. A., Ertl, C., Horneman, K., and Lovell, T. A. *Doppler-Only Initial Orbit Determination for an Orbiting Transmitter*.

[4] Waggoner, K., Curtis, D. H., and Little, B. "Analysis of TDOA/FDOA State Estimation Accuracy of Cislunar Objects for Space Situational Awareness." *IEEE Aerospace Conference*, 2023.

[5] Thompson, M. R., Popplewell, M. D., and Cheetham, B. "Utilization of Space-Based TDoA and FDoA for Cislunar Orbit Determination." *Advanced Maui Optical and Space Surveillance Technologies Conference (AMOS)*, 2022.

[6] Furfaro, R., Reddy, V., Campbell, T., and Gray, B. "Tracking Objects in Cislunar Space : The Chang'e 5 Case." *Advanced Maui Optical and Space Surveillance Technologies Conference (AMOS)*, 2021, pp. 0–6.

[7] Mušicki, D., and Koch, W. "Geolocation Using TDOA and FDOA Measurements." *Proceedings of the 11th International Conference on Information Fusion, FUSION 2008*, 2008. https://doi.org/10.1109/ICIF.2008.4632455.

[8] Guo, F., Fan, Y., Zhou, Y., Xhou, C., and Li, Q. "Space Electronic Reconnaissance: Localization Theories and Methods." *Space Electronic Reconnaissance: Localization Theories and Methods*, 2014, pp. 1–357. https://doi.org/10.1002/9781118542200.

[9] Kinzly, N., Polzine, B., Woodburn, J., and Short, C. *Simulating a Dynamics-Informed Cislunar RPO Mission Incorporating Orbit Determination*. Charlotte, North Carolina, 2022.

[10] Frnka, R. *The Circular Restricted Three-Body Problem*. Northern Arizonia University, 2010.

[11] Vallado, D. *Fundamentals of Astrodynamics and Applications*. Microcosm, Inc, Hawthorne, CA, 2013.

[12] Parker, J. S., and Anderson, R. L. *LOW-ENERGY LUNAR TRAJECTORY DESIGN*. 2013.

[13] Marchand, B. G., Howell, K. C., and Wilson, R. S. "An Improved Corrections Process for Constrained Trajectory Design in the N-Body Problem." *Journal of Spacecraft and Rockets*, Vol. 44, No. 4, 2007.

[14] Grebow, D. J. *Generating Periodic Orbits in the Circular Restricted Three-Body Problem with Applications to Lunar South Pole Coverage*. Purdue University, 2006.

[15] Frueh, C., Howell, K., Demars, K. J., Bhadauria, S., and Gupta, M. "Cislunar Space Traffic Management: Surveillance Through Earth-Moon Resonance Orbits." *8th European Conference on Space Debris*, Vol. 47907, No. May, 2021, pp. 20–23.

[16] Vauero, T. *Poincare Sections and Resonant Orbits in the Restricted Three-Body Problem*. Purdue Univercity, West Lafayett, Indiana, 2010.

[17] Deng, Z., Wang, H., Zheng, X., and Yin, L. "Base Station Selection for Hybrid TDOA/RTT/DOA Positioning in Mixed LOS/NLOS Environment." *Sensors (Switzerland)*, Vol. 20, No. 15, 2020, pp. 1–17. https://doi.org/10.3390/s20154132.

[18] National Aeronautics and Space Administration. *NASA Spacecraft Conjunction Assessment and Collision Avoidance Best Practices Handbook*. 2020.

[19] Channing, C., Ii, C., Jason, B., Wetterer, C. J., Dilley, M., Hill, K., Billings, P., Craft, C., and Frith, J. "Cislunar Orbit Determination: Improvements in Uncertainty Realism and Data Fusion." *Advanced Maui Optical and Space Surveillance Technologies Conference (AMOS)*, 2022.